

What the Milky Way’s Dwarfs tell us about the Galactic Center extended excess

Ryan E. Keeley,^{1,*} Kevork N. Abazajian,^{1,†} Anna Kwa,^{1,‡} Nicholas L. Rodd,^{2,§} and Benjamin R. Safdi^{3,¶}

¹*Department of Physics and Astronomy, University of California, Irvine, Irvine, CA 92697*

²*Center for Theoretical Physics, Massachusetts Institute of Technology, Cambridge, MA 02139*

³*Michigan Center for Theoretical Physics, Department of Physics, University of Michigan, Ann Arbor, MI 48109*

The Milky Way’s Galactic Center harbors a gamma-ray excess that is a candidate signal of annihilating dark matter. Dwarf galaxies remain predominantly dark in their expected commensurate emission. In this work we quantify the degree of consistency between these two observations through a joint likelihood analysis. In doing so we incorporate Milky Way dark matter halo profile uncertainties, as well as an accounting of diffuse gamma-ray emission uncertainties in dark matter annihilation models for the Galactic Center Extended gamma-ray excess (GCE) detected by the *Fermi Gamma-Ray Space Telescope*. The preferred range of annihilation rates and masses expands when including these unknowns. Even so, using two recent determinations of the Milky Way halo’s local density leave the GCE preferred region of single-channel dark matter annihilation models to be in strong tension with annihilation searches in combined dwarf galaxy analyses. A third, higher Milky Way density determination, alleviates this tension. Our joint likelihood analysis allows us to quantify this inconsistency. We provide a set of tools for testing dark matter annihilation models’ consistency within this combined dataset. As an example, we test a representative inverse Compton sourced self-interacting dark matter model, which is consistent with both the GCE and dwarfs.

PACS numbers: 95.35.+d,95.55.Ka,95.85.Pw,97.60.Gb

I. INTRODUCTION

The Large Area Telescope aboard the *Fermi Gamma-Ray Space Telescope*, *Fermi-LAT*, has observed a bright excess of gamma rays towards the Galactic Center whose presence is robust to systematic uncertainties in the standard background templates [1–12]. This excess has generated a great deal of interest since dark matter (DM) annihilation models can explain three compelling coincidences in the signal. First, the excess’ spatial morphology matches the predictions of a generalized Navarro-Frenk-White (NFW) profile, which is a generic prediction of cold DM models [13, 14]. Second, the total flux of the signal is well fit by the annihilation cross-section required by a thermal production scenario to generate the observed cosmological relic abundance. Third, the spectrum roughly matches the expectations of a tens of GeV weakly interacting massive particle (WIMP) annihilating to standard model particles. Should the GCE turn out to be explained by such an annihilating WIMP DM particle, it could be the first non-gravitational evidence of DM and the first strong clue of the particle nature of DM.

The prompt annihilation of WIMPs is not the only class of DM models that can explain the GCE, however. For example, a class of self-interacting DM (SIDM) models can explain the GCE via up-scattering of starlight that would not be seen in Dwarf galaxies [15–19]. Specif-

ically, this class of SIDM particles could annihilate into electrons (as well as the other standard model leptons) and these electrons could up-scatter the Galactic Center’s interstellar radiation field (ISRF) via the inverse Compton (IC) process.

There are also reasonable astrophysical interpretations of the GCE. Most notably is that the GCE can arise from a population of unresolved millisecond pulsars (MSP) [5, 7, 20–29]. Specifically, observations of MSPs in globular clusters show they have a spectrum consistent with the spectrum of the GCE. Further, low mass X-ray binaries (likely progenitors of MSPs) in M31 have been observed to follow a power law radial spatial distribution, similar to the expectations of an NFW halo [5, 25]. Other astrophysical explanations might include more dynamic events such as cosmic-ray injection into the Galactic Center (GC) [30–33]. Furthermore, the presence of the *Fermi* Bubbles tell us that such dynamic events have occurred in the past, so whatever mechanism produced the *Fermi* Bubbles, could also have produced the GCE [34–36].

There have arisen a number of independent avenues that each has the potential to challenge a DM interpretation of the GCE. One such avenue is to look for a gamma-ray excess from other DM halos. Such halos include those of galaxy clusters, the limits from which have recently been extended to be in slight tension with the GCE [37, 38], and the Milky Way’s satellite dwarf galaxies, the most recent *Fermi* limits appearing in Ref. [39]. Unfortunately, *Fermi-LAT* observations of both of these sources, and particularly the dwarfs, have not seen a significant complementary gamma-ray excess.¹ In particular, this difference between the GCE and the dwarfs

* rkeeley@uci.edu
† keverk@uci.edu
‡ akwa@uci.edu
§ nrodd@mit.edu
¶ bsafdi@umich.edu

¹ Note, however, there has been a low-significance detection of a

has the potential to rule out certain classes of DM interpretations of the GCE. Specifically, any minimal model based around a two-body annihilation process (any process where the flux is proportional to the square of the DM density) would exhibit this same tension.

Other avenues to test whether the GCE is better explained by annihilating DM or astrophysics is to more precisely check whether the morphology of the excess truly follows a smooth NFW profile. Tension in the morphology of the GCE has arisen from the detection of an ‘X-shape’ residual in the *Fermi* data which correlates infrared emission as seen by the WISE telescope [43]. Should this ‘X-shape’ template account for the entirety of the GCE, it would challenge any DM interpretation since DM annihilation would not produce such a shape. Measurements of the GCE being consistent with wavelets [44] or non-Poissonian fluctuations have also been reported [45–48], which would indicate an MSP rather than DM origin, though systematic uncertainties in such analyses remain [49]. Specifically, small scale gas clouds are left out of the model used by GALPROP, software used to generate the gamma-ray templates associated with cosmic rays propagating through the Milky Way, which could confuse any detection of point sources near the GC [49]. Though each of these lines of evidence against a DM interpretation of the GCE have their own systematic uncertainties, many of these systematics are independent of each other. Arguably, these different lines of evidence add up to strongly indicate that the GCE is astrophysical in origin.

Our focus in the present paper is to consider one aspect of this general line of reasoning: the consistency between the GCE and the dwarfs, and to do so with a more detailed treatment of the systematics coming from both sides. The discussion is structured as follows. In section II we discuss the background models we investigate to understand some of the dominant sources of systematic uncertainties in the problem. In section III, we discuss DM annihilation models of the GCE. In section IV, we discuss alternative models to promptly annihilating DM, including astrophysical interpretations and SIDM models. We conclude in section V.

II. BACKGROUND MODELS AND DATA

There remains significant uncertainty regarding the various processes that contribute to the gamma-ray signal coming from the GC. Any interpretation of the GCE will necessarily be affected by these uncertainties. To capture these effects, we investigate four different cases of the astrophysical background contributions to the GCE.

For all of our cases (denoted cases A, B, C, and D), we use data collected by *Fermi*-LAT. For cases A, B,

and C, that data corresponds to observations over a 103 month period from August 2008 to March 2017. We use all SOURCE-class photons from the Pass 8 instrument response functions. We apply a maximum zenith angle cut of 90° to avoid contamination. In cases A, B, and C, we focus our analysis on the innermost $7^\circ \times 7^\circ$ region of interest (ROI) about the Galactic Center. We then bin these photons into spatial bins of size $0.05^\circ \times 0.05^\circ$ for each energy bin. The photon events range from 200 MeV to 50 GeV and are binned in 16 logarithmically spaced energy bins.

For Case D we instead choose a dataset similar to that considered in the Inner Galaxy analyses of [11, 47]. Here we use the best quartile, as graded by the *Fermi* point spread function, of ULTRACLEANVETO-class Pass 8 photons, gathered between August 4, 2008 and June 3, 2016 with recommended quality cuts. This case can be contrasted with the above in that it generally corresponds to less data, but with less cosmic-ray contamination and improved angular reconstruction per event. To mimic an earlier Inner Galaxy analyses, we use a larger ROI of $30^\circ \times 30^\circ$, masking latitudes less than 1° . No masks were applied to the data in cases A-C. We also mask the top 300 brightest and most variable sources in the 3FGL catalog [50] at 95% containment. The photons are binned into 40 equally spaced logarithmic bins between 200 MeV and 2 TeV, and spatially using an `nside=128 HEALPix` grid [51].

With this processed data, we perform a maximum likelihood analysis to determine the best fit background model and GCE model. For each component of our model, we generate a template which encodes the spatial distribution of the photons for that component. The quantity that we are trying to determine is then the linear combination of these spatial templates that best fit the observed number of counts. The templates fall into three groups: point sources, extended emission, and diffuse emission. The point sources we use are taken from *Fermi*’s 3FGL point source catalog [50] and they are typically well characterized or independent of the GCE result. The extended emission components include a GCE template, as well as background components coming from cosmic rays interacting with gas in the interstellar medium (ISM) or photons in the ISRF. Specifically, these would include any IC radiation from high energy electron cosmic rays up-scattering the ISRF, neutral pion (π_0) decay generated from hadronic cosmic rays interacting with the ISM, and bremsstrahlung radiation arising from high energy electrons interacting with the ISM. The spatial distribution of these components are more *a priori* uncertain than point sources and are partially degenerate with the GCE, especially in the lowest energy bins, where the point-spread function is the largest. Therefore, it is these uncertainties and degeneracies that make a careful and broad investigation of the diffuse backgrounds crucial to analyzing the GCE and are the main difference between our different cases.

Since the uncertainty in the spectral shape of the GCE

gamma-ray excess from Reticulum II and Triangulum II, see e.g. [40, 41], although see also [42].

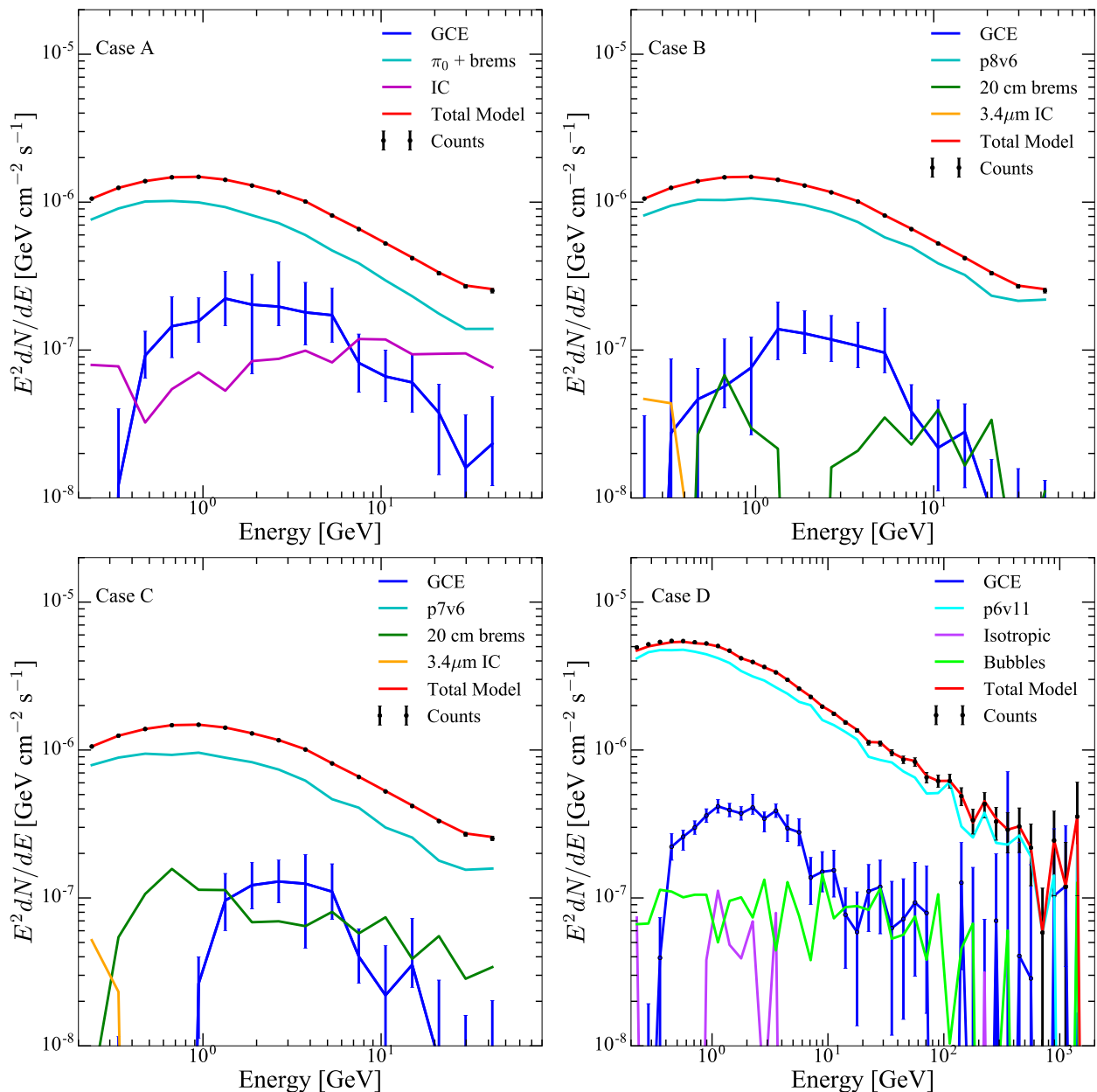


FIG. 1. Here we plot the energy flux spectrum (intensity) $E^2 dN/dE$ for the various templates included in the likelihood fits for our A, B, C, and D background cases. These show the total emission from the ROI, $7^\circ \times 7^\circ$ for cases A-C and $30^\circ \times 30^\circ$ for case D. The error bars on the counts is the Poisson error. The various 3FGL sources were also varied in the fits but are not included for the sake of simplicity.

signal is dominated by systematic uncertainties in the background templates, rather than Poisson fluctuations of the total counts, it is necessary to explore multiple possible background models. To this end, we use four different sets of templates for these extended background models:

- **Case A:** We use the templates for the π_0 , bremsstrahlung, and IC emission for ‘model F’ from Horiuchi et al. (2016) [49], which in turn

used diffusion model parameters from Calore et al. (2014) [12] to generate their background models. Their ‘model F’ corresponds to the diffuse background model that was found to best fit the data in their ROI. Unlike the *Fermi* collaboration Pass 8 and Pass 7 diffuse backgrounds, the IC component of the diffuse background is fit independently of the π_0 +bremsstrahlung components. We used the templates for ‘model F’ from these papers. In this work, we denote this ‘case A.’

- **Case B:** For this case, we use the Pass 8 Galactic interstellar emission model from the *Fermi* tools, which models the distribution of gamma rays coming from π_0 decay, bremsstrahlung, and IC. All three components are combined in a single diffuse template with fixed relative normalizations in each energy bin. Furthermore, we used a template which traces the 20 cm radio emission first discovered by Yusef-Zadeh et al. (2013) [52]. We also include a template for an additional IC component that was derived from $3.4\mu\text{m}$ maps from the WISE telescope, discovered by Abazajian et al (2014) [10].
- **Case C:** This case uses the same templates for the bremsstrahlung and IC components but uses p7v6 model for Pass 7.
- **Case D:** This case uses the p6v11 template and floats an isotropic template as well as a template for the *Fermi* bubbles.

For all these cases, we allow the flux associated with each template in a given bin to be independent of the flux in other bins, rather than assume a specific component has a specific spectral shape. This allows us to be agnostic about the shape of the spectrum for each of these sources, but potentially comes at the cost of over-fitting the data. The results of these maximum likelihood fits for cases A-D are shown in Fig. 1.

To calculate posteriors for the dwarfs, we use the flux likelihood limits from Albert et al. (2016) [39]. Specifically, we use the flux likelihood manifolds for the twenty kinetically confirmed dwarf galaxies that have measured J-factors. To calculate these flux likelihood limits, Albert et al. use six years of LAT data with 24 equally-spaced logarithmic bins between 500 MeV and 500 GeV. They binned the photons in a $10^\circ \times 10^\circ$ region about the target dwarf galaxies with a pixel size of 0.1° in order to model any overlap from the points spread function of the point sources in the 3FGL catalog, from the Galactic diffuse emission, and from the isotropic model. Each target dwarf galaxy was modeled as a point-like source and used a maximum likelihood analysis with these templates to generate the flux likelihood limits.

III. ANNIHILATING DARK MATTER MODELS

A. Flux Spectra

The differential flux in some ROI for the class of two-body DM annihilation is given by the following:

$$\frac{d\Phi}{dE} = \frac{1}{4\pi} \frac{J}{m_\chi^2} \frac{\langle\sigma v\rangle}{2} \frac{dN}{dE}. \quad (1)$$

Here, J is the J-factor, the integral of the density-squared over the ROI and through the line of sight. m_χ is the mass of the DM particle and $\langle\sigma v\rangle$ is the thermally averaged cross section of the annihilation. $\frac{dN}{dE}$ is

the per-annihilation spectrum, which we calculated using PPPC4DMID [53]. For our dark matter models, we use flat priors on the DM mass and scale invariant priors on the cross section. The prior on the J-factor is discussed in the next section.

B. J-factors

The J-factor is the square of the DM density integrated through the line of sight and integrated over the ROI.

$$J = \int_{\text{ROI}} d\Omega \int dz \rho^2(r(z, \Omega)). \quad (2)$$

As in Abazajian & Keeley 2015 [54], we determine the prior on the J-factor for the GC by parameterizing the Milky Way's DM halo as a generalized NFW profile with a local DM density (ρ_\odot), a scale radius (R_s), and an inner profile slope (γ)

$$\rho(r) = \frac{\rho_\odot}{\left(\frac{r}{R_\odot}\right)^\gamma \left(\frac{1+r/R_s}{1+R_\odot/R_s}\right)^{3-\gamma}}. \quad (3)$$

Each of these parameters has a probability distribution, so in principle, we could say the prior on the J-factor is the product of the probability distributions of each of these parameters and then perform the change of variables to write this probability distribution as a function of the J-factor. This is analytically cumbersome, so we use numerical Monte Carlo methods to calculate this distribution. Specifically, we draw values for the local density, scale radius, and inner slope to compute a set of J-factors and then use kernel density estimation to define the prior for the GCE J-factor.

For the local density, we use the value determined by Zhang et al (2012) [55]: $\rho_\odot = 0.28 \pm 0.08 \text{ GeV cm}^{-3}$. This robust determination of the local DM density is derived from modeling the spatial and velocity distributions for a sample of 9000 K-Dwarf stars from the Sloan Digital Sky Survey (SDSS). The velocity distribution of these stars directly measures the local gravitational potential and, when combined with stellar density constraints, provides a measure of the local DM density.

The prior on the scale radius is calculated from the concentration, which is the ratio of the virial radius to the scale radius. The uncertainty in the concentration is calculated from simulations of galaxy formation. Sanchez-Conde and Prada (2013) [56] parameterized the uncertainty in the concentration of a DM halo as a function of that halo's mass. Thus we can write the prior on the scale radius as:

$$\log \mathcal{L} = -\frac{(\log_{10}(R_{\text{vir}}/R_s) - \log_{10} c(M_{\text{vir}}))^2}{2 \times 0.14^2}. \quad (4)$$

The prior on the inner slope we use for the Monte Carlo calculation of the J-factor is taken to be the posterior determined by the spatial information contained

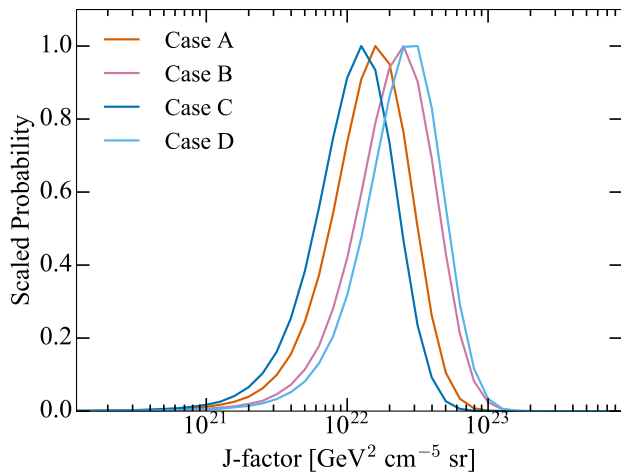


FIG. 2. The prior on the J-factor integrated over the ROI derived through a Monte Carlo convolution of the priors on the local density, scale radius, and inner slope. Since each of the different background cases have different best fit values for γ , and since case D corresponds to a larger ROI, the derived uncertainties on the J-factors are different.

in the GCE data. We constrain the inner slope by running the likelihood analysis with the same background models but with different NFW spatial templates that have different values for the inner slope. The likelihood analysis calculates the $\Delta\text{Log-likelihood}$ value for each of these different cases, which allows us to fit a χ^2 distribution to these $\Delta\text{Log-likelihood}$ values. This determines the best fit value of γ and its error. Unsurprisingly, this derived prior on the inner slope depends on the background model used. For case A we calculate, $\gamma = 1.14 \pm 0.04$; for case B, $\gamma = 1.24 \pm 0.04$; for case C, $\gamma = 1.10 \pm 0.04$; and for case D, we calculate $\gamma = 1.2 \pm 0.06$. The results of this Monte Carlo calculation of the priors on the J-factor for the different background cases is shown in Fig. 2.

We employ the priors on the J-factors for the dwarf galaxies from Albert et al. (2016) [39]. These are all reported as log-normal distributions. These J-factors come with some caveats, however. Specifically, assumptions about how spherically symmetric the dwarf galaxy is, which in turn can influence the inferred cuspidity of the density profile, can lead to systematic uncertainties greater than the statistical uncertainties [57–59].

C. Evidence Ratios

To quantify the tension between the GCE and the dwarfs, we calculate a Bayesian evidence ratio. This evidence ratio can be used in answering the question: by what factor do the odds of some model being true change with the inclusion of a new data set. It is the product of the Bayesian evidences of two data sets, D_1 and D_2 , when considered separately divided by the evidence of

the two data sets when considered jointly [60]:

$$\begin{aligned} \text{ER} &= \frac{p(D_1)p(D_2)}{p(D_1, D_2)} \\ &= \frac{\int d\theta_1 p(D_1|\theta_1)p(\theta_1) \int d\theta_2 p(D_2|\theta_2)p(\theta_2)}{\int p(D_1, D_2|\theta)p(\theta)}. \end{aligned} \quad (5)$$

This can be interpreted as a Bayes factor where the two models being compared are the same except for the fact that the model corresponding to the numerator has an additional, independent copy of the parameter space and the two parameter spaces describe the two data sets separately.

This statistic can indicate three different outcomes for the model. First, if the data set D_2 contains no information, then this evidence ratio is unity. If D_2 is entirely consistent with D_1 then the evidence ratio should be less than unity. This is expected since increasing the complexity of a model should come at a cost of subjective belief. If D_2 is in tension with D_1 then this evidence ratio will be greater than unity. How strongly this evidence ratio prefers consistency or tension can be interpreted by any standard Bayes factor scale. In this work, we choose to interpret our evidence ratios by the Jeffreys’ scale.

Using this setup, we then calculate evidence ratios between the combined dwarf galaxies and the GC. The results are stated in Table I.

One particularly useful feature of evidence ratios in this context is that, compared to Bayes factors, they are relatively insensitive to systematic uncertainties in the background models. These systematic uncertainties can alter the total flux of the signal, but they more drastically change in which energy bin this flux is distributed. This is seen most clearly in the lowest energy bins, where the inclusion of diffuse templates from 20 cm maps of bremsstrahlung emission and 3.4 μm maps of IC emission, for cases B and C, remove all the photons from the NFW template for these bins. Such changes to the lowest energy bins changes the overall curvature of the GCE spectrum, which, in turn, significantly changes the best fit mass but not the best fit cross section [54]. When the best fit mass of the GCE changes, the amount of overlap between the GCE posterior with the combined dwarfs posterior (and hence the evidence ratio) changes relatively little. This lack of change in overlap comes from the fact that the contours of the dwarf posterior are almost parallel to contours of constant cross section, since the lack of a dwarf signal contains no significant amount of information about the spectrum. It is because the evidence ratio is most sensitive to the cross section and not particularly sensitive to the dark matter mass that the evidence ratios are more robust to systematic uncertainties in the background templates. This is born out in Table I where the DM evidence ratios for the different cases vary by only two orders of magnitude. On the other hand, because the Bayes factors are sensitive to both the normalization and the shape of the spectrum it can vary by 30 orders of magnitude, as seen in Table

TABLE I. Evidence ratios for our five models using the diffuse templates for our various background cases.

Model	Case A	Case B	Case C	Case D
DM: $b\bar{b}$	3600	21	220	15
DM: $\tau^+\tau^-$	2300	25	230	29
Log-Parabola	0.69	0.58	0.71	0.54
Exponential Cutoff	0.73	0.59	0.78	0.54
SIDM	1.1	1.2	1.2	1.1

II.

Beyond systematic uncertainties due to the inclusion of additional templates for bremsstrahlung and inverse Compton processes, uncertainties in the diffuse model for the GALPROP generated π_0 , IC, and bremsstrahlung templates, can alter the total flux of the GCE signal and will affect the best fit cross section for the GCE and hence affect the tension with the dwarfs. This is seen by the fact the evidence ratio for our different cases significantly change. This change is caused by the fact that the differences in these diffuse emission templates, for cases B and D, shift the overall flux of the GCE signal to smaller values, relative to case A. In these background model cases, the presence of the GCE is less significant and reduces the significance of the tension with the dwarfs.

The information encoded by the evidence ratio can be qualitatively seen in Fig. 3, which plots the posterior of our $b\bar{b}$ and $\tau^+\tau^-$ DM annihilation models for each of our different GCE background cases and for the dwarf data. The amount of overlap in the GCE posteriors and the dwarf posterior indicates the amount of tension between the data sets.

For our DM annihilation models, we calculate evidence ratios between 15 and 2200 for the $b\bar{b}$ channel and between 27 and 4300 for the $\tau^+\tau^-$ channel. Using the Jeffreys Scale, this indicates a strong (>10) to decisive (>100) tension in two-body DM interpretations of the GCE and dwarf data.

Importantly, this strong to decisive tension exists in models beyond just the specific DM particle annihilating to $b\bar{b}$ or $\tau^+\tau^-$. Any model of prompt two-body decay, described by a J-factor, would exhibit this same tension. Hence, models that contain only novel versions of spectrum dN/dE , or branching ratios, will not alleviate this strong tension.

D. Caveats

The GCE-dwarf tension we quantified in the previous section certainly depends on the prior information adopted for the J-factors of the GC region and the dwarf galaxies. Naturally, if there was a significant change in the inferred DM content of either the GC region or dwarf galaxies, then the nature of tension would correspond-

ingly change. However, our choices for the J-factor of the GC region and dwarf galaxies are those determined by the most robust analyses available.

The parameter that the J-factor is most sensitive to is the local density of DM. As stated in a previous section, we use a value of 0.28 ± 0.08 GeV/cm³ taken from Zhang et al. (2012) [55]. Other groups including Pato et al. (2015) [61] and McKee et al. (2015) [62] tend to find higher values for the local density. To fully resolve the tension between the GCE and the dwarfs, the GCE J-factor needs to increase between 1 and 1.5 orders of magnitude, which translates into a local density of 3 to 6 times greater. As we show, none of these determinations of the local density relieve the GCE-dwarf evidence ratio to be unity.

Another parameter with a systematic uncertainty is the scale radius of the DM profile. Small deviations around our fiducial value would not change the J-factor by a great deal since the inner profile is unchanged due to the scale radius being beyond the local radius. However, should the scale radius become smaller than the local radius, the inner density profile would increase as r^{-3} between the local radius and the scale radius, resulting in a larger J-factor. A profile with such a small scale radius could only occur in halos with a concentration parameter far outside of what CDM simulations predict for halos with the mass of the Milky Way.

The inner slope γ is more robust to systematic uncertainties, in that it is determined directly from the spatial information of the gamma-ray data. In particular, to fully resolve the GCE-dwarf tension, a value of around $\gamma = 1.7$ would be required. However, all of the diffuse models that we tested preferred values for the inner slope were found to be significantly below that, between and $\gamma = 1.1$ and 1.3. Despite systematic uncertainties in the parameterization of the Milky Way's DM profile, no single alteration can fully relieve the tension between the GCE and dwarf data.

IV. MODELS

We have shown that there is tension with the standard WIMP scenario between the derived cross sections from the GC and the dwarfs, with some important caveats. This tension can potentially point to alternate models being better explanations for the GCE, including astrophysical interpretations to more complicated DM models. To quantitatively answer this question, we calculate a Bayes factor:

$$K_{12} = \frac{p(M_1|D)p(M_2)}{p(M_2|D)p(M_1)} = \frac{p(D|M_1)}{p(D|M_2)}. \quad (6)$$

We consider the following models: two astrophysical interpretations, one with a log-parabola spectrum and another with an exponential cutoff spectrum, and a SIDM model where the GCE gamma rays are generated by DM

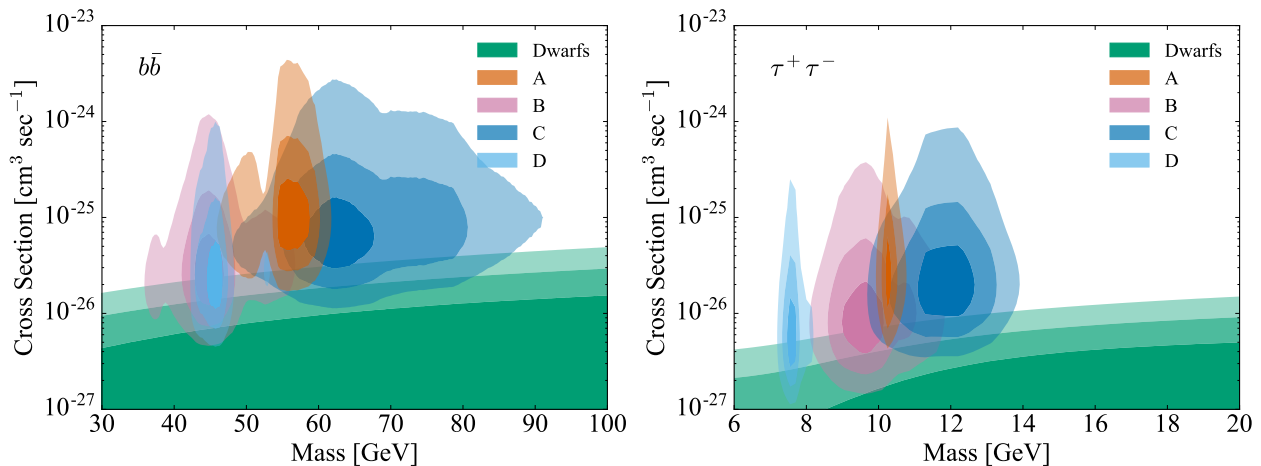


FIG. 3. Here we show the 1, 2, and 3σ contours of the posteriors for the annihilation cross section and DM mass. Our calculated limits on the dwarf signal is in green, case A is in orange, case B is in blue, and case C is in pink. The results for $b\bar{b}$ on the left and $\tau^+\tau^-$ on the right. The amount of overlap qualitatively demonstrates the information contained in the evidence ratio and shows how consistent two-body DM annihilation models are at explaining both the GCE and the lack of a dwarf signal.

decaying to high-energy electrons up-scattering starlight. The Bayes factors for our models are given in Table II.

A. Astrophysical Interpretations

Should the GCE have an astrophysical interpretation, the gamma-ray spectrum can be parameterized as a log-parabola or a power law with an exponential cutoff. We investigate both parameterization as explanations of the GCE.

The spectrum for our log-parabola model is given by:

$$\frac{dN}{dE} = N_0 \left(\frac{E}{E_s} \right)^{-\alpha - \beta \log(E/E_s)}, \quad (7)$$

where N_0 is an arbitrary normalization, E_s is a scale energy, α is the slope of the power-law part of the spectrum, and β parameterizes the turnover of the spectrum.

The spectrum for our power law with an exponential cutoff model is given by:

$$\frac{dN}{dE} = N_0 \left(\frac{E}{E_s} \right)^\gamma e^{-E/E_c}, \quad (8)$$

where N_0 is the normalization of the spectrum, E_s is a scale energy, γ is the slope of the power-law part of the spectrum, and E_c parameterizes how fast the spectrum cuts off.

Our astrophysical models do not have a specific physical interpretation so it is not straightforward to investigate to what extent the GCE and the lack of signal from the dwarf galaxies are compatible given these models. Presumably, if the GCE and any potential dwarf signal were to be explained by the same category of astrophysical object, then they should have the same spectral

parameters. Therefore, it makes sense for our model to have only one set of spectral parameters that describes both the GCE and the dwarfs. The normalizations of the spectrum, however, would not necessarily be the same. One option is to allow the normalization of the spectrum of the GCE and the spectrum of each of the dwarfs to be independent. Following this parameterization, we calculate an evidence ratio between the GCE and the dwarfs of about 1, which would indicate the two data sets contain no new information relative to each other. This is expected, since if we put in the fact that the signals are independent, we should get out that they have no mutual information. Instead of saying these normalizations are entirely independent of each other, we use a zeroth order ansatz to parameterize the normalization as the product of the stellar mass of the system and the gamma-ray rate per stellar mass. The stellar mass would, of course, be independent between regions, but the gamma-ray rate per stellar mass should be the same between regions. To this end, we find N_0 in the above equations such that the integral of dN/dE over our energy range (200 MeV to 50 GeV) is one. This allows us to attach physical interpretations to our normalization for $d\Phi/dE$.

Specifically, it makes sense, should the initial mass function of some galaxy be independent of the stellar mass of that galaxy, that the gamma-ray production rate scales linearly with the stellar mass of the galaxy. Hence, the gamma-ray rate per stellar mass should be consistent across all regions.

Ultimately, this leads to the following parameterization of the differential number flux:

$$\frac{d\Phi}{dE} = \frac{\dot{N}}{4\pi R^2} \frac{M_*}{M_0} \frac{dN}{dE}, \quad (9)$$

where M_* is the stellar mass of the object, R is the distance to the object, and \dot{N}/M_0 is the gamma-ray rate per

stellar mass, which should be the same between different objects.

For both spectra of astrophysical models, we marginalized over the spectral parameters with flat priors, and marginalized over the over the gamma-ray rate per stellar mass with a scale invariant prior. We use the stellar mass of the dwarfs, the distance to them, as well as the uncertainties in those parameters from McConnachie (2012) [63]. Interestingly, both of our astrophysical models pick out values for the gamma-ray rate per stellar mass around $10^{31\pm1} \text{ s}^{-1} M_{\odot}^{-1}$, which is consistent with known millisecond pulsars. In the end, the evidence ratios for each of our two spectral choices for astrophysical models, for all of our background cases, are less than unity. Importantly, this less than unity evidence ratio indicates that the combined dwarf and GCE data have a weak indication of a mutual astrophysical excess described by a single set of parameters.

The Bayes factors we compute also point towards a preference for these astrophysical models. As seen in Table II, the log-parabola spectrum is preferred over any DM model in each of the cases, and the exponential cutoff spectrum is preferred in three out of four of the cases. The preference in the Bayes factor can be thought of as coming from two distinct sources. One is the GCE data on their own prefer that model and the other is that the model can better explain the differences in the flux from the GC and the dwarfs. Astrophysical interpretations, with evidence ratios less than unity, can do better on the latter count, but interestingly, depending on the data case, can also do better on the former count. In all cases, the log-parabola spectrum can explain the GCE data better than dark matter models, but in cases B and C, the exponential cutoff can do so also. This preference in some cases for the log-parabola spectrum is predominantly coming from the lowest energy bins. The maximum likelihood fit prefers giving no appreciable amount of photons to the lowest energy bins, a fact that is difficult for DM models to explain, but is more easily accommodated by the log-parabola spectra. This preference of the lowest energy bins for the log-parabola spectra can be seen in Figure 4, where we plot the best fit models, along with the data. It is worth noting that these lowest energy bins have the largest systematics associated with them due to the large size of the size of the point spread function at those energies [12]. Unlike the evidence ratios, the Bayes factors are particularly sensitive to these systematics, particularly because no model is a strikingly good fit, just less bad than the others. Indeed, when ignoring the first few data points for each data case, the Bayes factors tend to show less extreme results, giving more consistent fits to the GCE. With these truncated data sets, the values of the Bayes factors come from the models' abilities to explain the difference in flux coming from the GC and the dwarfs.

On an additional note, the preference for $b\bar{b}$ can also be seen in Fig. 4. Since the $\tau^+\tau^-$ model requires a light (compared to the $b\bar{b}$ model) dark matter mass to explain

the peak of the GCE spectra at around 1-2 GeV, and since these annihilating dark matter models cutoff in energy at around their mass, the $\tau^+\tau^-$ model fail to account for the GCE spectra that gradually fall off with large energies, such as in cases A, B, and D.

B. A Representative SIDM Model

In certain classes of SIDM models for the GCE, the gamma-ray excess is generated by the DM particles annihilating to electron-positron pairs through a light mediator [15]. The electrons then up scatter the starlight in the Galactic Center via an IC process. This would naturally explain the difference in the observed gamma-ray flux between the GC and the dwarfs since the stellar density of the dwarfs, and therefore the interstellar light, is many orders of magnitude smaller than the stellar mass of the GC.

Should the GCE be explained DM annihilating to electrons that interact with the ambient starlight, the process should be governed by the following IC equation:

$$\frac{dn_{\gamma}}{dEdt} = \sigma_T c n_e n_{\text{ISRF}} \frac{dN_{\gamma}}{dE}, \quad (10)$$

where n_{γ} is the number density of gamma rays, σ_T is the Thomson cross section, n_e is the number density of electrons produced by annihilating DM, n_{ISRF} is the number density of low energy photons in the interstellar radiation field, and $\frac{dN_{\gamma}}{dE}$ is the probability distribution function of producing a gamma ray of energy E via this IC process. Naturally, this probability distribution function depends on the probability distribution functions of the energies of the electrons produced via DM annihilation and the energy distribution of the starlight:

$$\frac{dN_{\gamma}}{dE} = \int dE_e dE_{\text{ISRF}} p(E_{\gamma}|E_e, E_{\text{ISRF}}) p(E_e) p(E_{\text{ISRF}}). \quad (11)$$

In principle, other energy-loss mechanisms, such as synchrotron emission, can alter the energy distribution of electrons in this IC process. We checked this model against the spectrum PPPC4DMID calculates and found the shape of the spectra were largely consistent.

Since the electrons are produced via a two-body interaction, the number density of electrons should scale as the square of the number density of DM particles: $n_e \propto n_{\chi}^2$. To convert the time derivative of the differential number density of photons to some number flux, we need to evaluate the following integral:

$$\frac{d\Phi_{\gamma}}{dE} = \int dV' \frac{1}{4\pi(\vec{R} - \vec{R}')^2} \frac{dn_{\gamma}}{dEdt}(\vec{R}'). \quad (12)$$

Choosing the origin of the coordinate system to be at $R = 0$ leads to the standard expression for the J-factor, should the process be entirely a two-body process and

the time derivative of n_γ scale solely as the square of the DM particles. Putting this all together, we get:

$$\frac{d\Phi_\gamma}{dE} \propto \int d\Omega dz \frac{1}{4\pi} n_{\text{ISRF}} n_\chi^2 \frac{dN}{dE}. \quad (13)$$

Instead of using this equation as written, we make the following assumptions and simplifications. First, n_{ISRF} is approximately constant where the density of DM is largest, so we can pull the factor of n_{ISRF} outside the integral. Second, it should be true that the number density of photons from stars scales with the stellar mass of those stars we replace n_{ISRF} with the stellar mass of the gamma-ray source, M_* :

$$\frac{d\Phi_\gamma}{dE} \propto \frac{J}{m_\chi^2} \frac{M_*}{M_{*,\text{GC}}}. \quad (14)$$

Taking this spectrum leads to a model that has far greater consistency between the GCE and dwarfs; the evidence ratios for this model are all around unity for each of the data cases. This highlights the possibility to alleviate the tension when going beyond simple two-body final state scenarios.

The best fit DM mass for this representative SIDM model is 15 ± 1 GeV for cases A and D, 15 ± 3 GeV for case B, and 21 ± 2 GeV for case C.

To construct a more realistic and self-consistent SIDM model, we would need to account for two effects. The first is Sommerfeld enhancement in the dwarfs. This Sommerfeld enhancement causes an increase in the effective annihilation cross section due to the smaller velocity dispersion in the dwarfs, relative to the GC [15]. This would tend to push down the limits on the DM annihilation cross section coming from the dwarfs. However, unless this enhancement factor were many orders of magnitude above unity, the evidence ratio would still be around unity. The second effect would have the opposite impact on the dwarfs' cross section limits. Since SIDM models generically predict cored density profiles for the dwarfs [64], the inferred central density of the dwarves would be smaller than implied by assuming an NFW profile, as is currently done. This, in turn, would decrease the J-factors of the dwarfs and push up the limits on the DM annihilation cross section.

V. CONCLUSIONS

We have analyzed the GCE in a wide variety of background models by performing a template based likelihood analysis of the GC using four different models for the diffuse background templates. To answer the question of whether an annihilating DM interpretation can be consistent with the lack of dwarf signals, we calculated evidence ratios for each model of the GCE and for each case of diffuse background models. These evidence ratios are sensitive to the choice of background model but they all display strong to decisive tension between the GCE

TABLE II. Bayes factors for the considered models, relative to the $b\bar{b}$ model, for each of the different background cases. Values larger than one indicate the data prefer that model over $b\bar{b}$.

Model	Case A	Case B	Case C	Case D
DM: $\tau^+\tau^-$	4×10^{-24}	1×10^{-5}	7×10^4	1×10^{-22}
Log-Parabola	3×10^{12}	4×10^5	2×10^{12}	5×10^9
Exponential Cutoff	2×10^1	2×10^4	4×10^{10}	0.1
SIDM	5×10^{-20}	8×10^{-19}	6×10^{-2}	0.1

and the dwarfs for annihilating DM models. Specifically, cases A and C show decisive tension, with evidence ratios greater than 100 for both annihilation channels, and cases B and D show strong tension with evidence ratios greater than 10 for both channels. This difference can, at least in part, be attributed to the fact the likelihood fit for these cases seem to prefer both giving less flux to the DM GCE component, and also prefer an NFW template with a higher value for the inner slope γ . Since the tension is seen to various degrees using a variety of models for the the diffuse emission, it is robust to say that prompt two-body annihilating DM interpretations of the GCE are in strong doubt.

Astrophysical and SIDM interpretations of the GCE fare better with evidence ratios around unity. Ultimately, allowing the gamma ray signal to scale with the stellar mass, as for astrophysical models, or with the product of the J-factor and stellar mass, as with SIDM models, relieves any tension between the GCE signal and lack of a dwarf signal.

We also calculated Bayes factors for our different DM GCE interpretation models. This Bayes factor can be thought of as coming from two different sources: the ability of the model to explain the GCE and the ability of the model to explain the difference in GCE and dwarf fluxes. These Bayes factors decisively prefer the log-parabola spectrum model over the DM annihilation models in all of our background cases, and prefer the exponential cutoff model in three of the four background cases. This preference for either astrophysical spectrum model predominantly comes from the lowest energy bins where the likelihood analysis prefers to attribute no amount of flux to an NFW template. However, these are also the energy bins that have the largest systematic uncertainties associated with them. Standard two-body DM annihilation models cannot explain these low energy gamma-ray data, while more general log-parabola and exponential cutoff models are able to do so. With the long integration time now available from the *Fermi*-LAT observations of the GCE, the data allows us to make very precise determinations of the GCE's spectral parameters, given a particular background model. However, the accuracy of these background models are still uncertain. In other

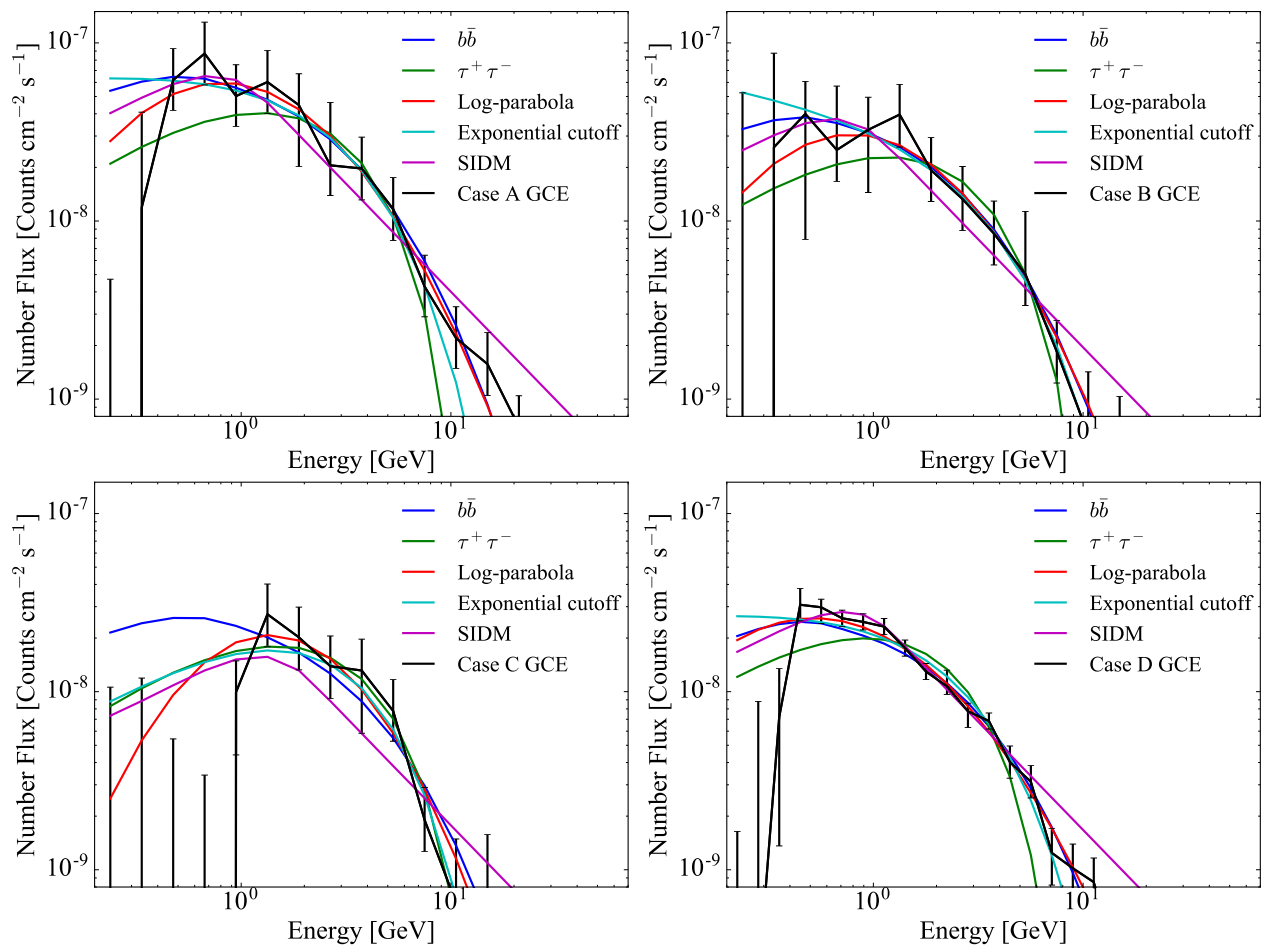


FIG. 4. Here we plot the number flux for the GCE template along with the best fit spectra for the different models considered. The error bars correspond to the 1- σ region of each bin's number flux likelihood profiles.

words, the systematic uncertainties in the background model cases dominate over the Poisson statistical uncertainties. In fact, there exist two sets of tests. One is whether DM or astrophysical spectral models' can explain the joint GCE and dwarf data. The second is the intrinsic ability of the GCE spectral choices to explain the GC observations. Importantly, the biggest change in the models' Bayes factors comes from the spectral models' different ability to properly fit the GCE. In almost all cases, log-parabola spectra is decisively better in their evidence ratios at fitting the GCE data (cf. Table II). Therefore, given the GCE data alone, the log-parabola astrophysical interpretation of the GCE is favored.

Furthermore, the combined GCE-dwarf data strongly to decisively disfavor single channel DM annihilation interpretations of the GCE. Secondary-emission from DM models like that from SIDM could alleviate the inconsistent emission between the GCE and dwarf galaxies.

Further detailed analysis of the diffuse emission towards the GC will help determine the true nature of the GCE and its relation to any emission from the dwarf galaxies.

ACKNOWLEDGMENTS

K.N.A. and R.E.K. are supported in part by NASA *Fermi* GI grant 15-FERMI15-0002. A.K. is supported by NSF GRFP Grant No. DGE-1321846. N.L.R. is supported by the DOE under contracts DESC00012567 and DESC0013999. We thank Dan Hooper, Manoj Kaplinghat and Savvas Koushiappas for useful discussions. We also thank Barbara Szczerbinska and the other organizers of *XI International Conference on Interconnections between Particle Physics and Cosmology*, in Corpus Christi, Texas, where part of this collaborative work was initiated.

[1] L. Goodenough and D. Hooper, (2009), arXiv:0910.2998 [hep-ph].

[2] V. Vitale and A. Morselli (Fermi-LAT), in *Fermi gamma-ray space telescope. Proceedings, 2nd Fermi Sympo-*

- sium, Washington, USA, November 2-5, 2009* (2009) arXiv:0912.3828 [astro-ph.HE].
- [3] D. Hooper and L. Goodenough, *Phys.Lett.* **B697**, 412 (2011), arXiv:1010.2752 [hep-ph].
 - [4] D. Hooper and T. Linden, *Phys.Rev.* **D84**, 123005 (2011), arXiv:1110.0006 [astro-ph.HE].
 - [5] K. N. Abazajian and M. Kaplinghat, *Phys.Rev.* **D86**, 083511 (2012), arXiv:1207.6047 [astro-ph.HE].
 - [6] C. Gordon and O. Macias, *Phys.Rev.* **D88**, 083521 (2013), arXiv:1306.5725 [astro-ph.HE].
 - [7] O. Macias and C. Gordon, *Phys. Rev.* **D89**, 063515 (2014), arXiv:1312.6671 [astro-ph.HE].
 - [8] D. Hooper and T. R. Slatyer, *Physics of the Dark Universe* **2**, 118 (2013), arXiv:1302.6589 [astro-ph.HE].
 - [9] K. N. Abazajian, N. Canac, S. Horiuchi, and M. Kaplinghat, *Phys.Rev.* **D90**, 023526 (2014), arXiv:1402.4090 [astro-ph.HE].
 - [10] K. N. Abazajian, N. Canac, S. Horiuchi, M. Kaplinghat, and A. Kwa, *JCAP* **1507**, 013 (2015), arXiv:1410.6168 [astro-ph.HE].
 - [11] T. Daylan, D. P. Finkbeiner, D. Hooper, T. Linden, S. K. N. Portillo, N. L. Rodd, and T. R. Slatyer, *Phys. Dark Univ.* **12**, 1 (2016), arXiv:1402.6703 [astro-ph.HE].
 - [12] F. Calore, I. Cholis, and C. Weniger, *JCAP* **1503**, 038 (2015), arXiv:1409.0042 [astro-ph.CO].
 - [13] J. F. Navarro, C. S. Frenk, and S. D. M. White, *Astrophys. J.* **462**, 563 (1996), arXiv:astro-ph/9508025 [astro-ph].
 - [14] J. F. Navarro, C. S. Frenk, and S. D. M. White, *Astrophys. J.* **490**, 493 (1997), arXiv:astro-ph/9611107 [astro-ph].
 - [15] M. Kaplinghat, T. Linden, and H.-B. Yu, *Phys. Rev. Lett.* **114**, 211303 (2015), arXiv:1501.03507 [hep-ph].
 - [16] M.-Y. Cui, C. Zhang, and H.-S. Zong, *Phys. Rev.* **D93**, 123516 (2016), arXiv:1605.08138 [hep-ph].
 - [17] T. Lacroix, O. Macias, C. Gordon, P. Panci, C. Bhm, and J. Silk, *Phys. Rev.* **D93**, 103004 (2016), arXiv:1512.01846 [astro-ph.HE].
 - [18] T. Lacroix, C. Boehm, and J. Silk, *Phys. Rev.* **D90**, 043508 (2014), arXiv:1403.1987 [astro-ph.HE].
 - [19] I. Galon, A. Kwa, and P. Tanedo, *JHEP* **03**, 064 (2017), arXiv:1610.08060 [hep-ph].
 - [20] K. N. Abazajian, *JCAP* **1103**, 010 (2011), arXiv:1011.4275 [astro-ph.HE].
 - [21] H. Ploeg, C. Gordon, R. Crocker, and O. Macias, *JCAP* **1708**, 015 (2017), arXiv:1705.00806 [astro-ph.HE].
 - [22] M. Ajello *et al.* (Fermi-LAT), Submitted to: *Astrophys. J.* (2017), arXiv:1705.00009 [astro-ph.HE].
 - [23] N. Mirabal, *Mon. Not. Roy. Astron. Soc.* **436**, 2461 (2013), arXiv:1309.3428 [astro-ph.HE].
 - [24] J. Petrovi, P. D. Serpico, and G. Zaharijas, *JCAP* **1502**, 023 (2015), arXiv:1411.2980 [astro-ph.HE].
 - [25] Q. Yuan and B. Zhang, *JHEAp* **3-4**, 1 (2014), arXiv:1404.2318 [astro-ph.HE].
 - [26] Q. Yuan and K. Ioka, *Astrophys. J.* **802**, 124 (2015), arXiv:1411.4363 [astro-ph.HE].
 - [27] T. D. Brandt and B. Kocsis, *Astrophys. J.* **812**, 15 (2015), arXiv:1507.05616 [astro-ph.HE].
 - [28] R. M. O'Leary, M. D. Kistler, M. Kerr, and J. Dexter, (2015), arXiv:1504.02477 [astro-ph.HE].
 - [29] R. M. O'Leary, M. D. Kistler, M. Kerr, and J. Dexter, (2016), arXiv:1601.05797 [astro-ph.HE].
 - [30] E. Carlson and S. Profumo, *Phys.Rev.* **D90**, 023015 (2014), arXiv:1405.7685 [astro-ph.HE].
 - [31] D. Gaggero, M. Taoso, A. Urbano, M. Valli, and P. Ullio, *JCAP* **1512**, 056 (2015), arXiv:1507.06129 [astro-ph.HE].
 - [32] I. Cholis, C. Evoli, F. Calore, T. Linden, C. Weniger, and D. Hooper, *JCAP* **1512**, 005 (2015), arXiv:1506.05119 [astro-ph.HE].
 - [33] E. Carlson, T. Linden, and S. Profumo, *Phys. Rev.* **D94**, 063504 (2016), arXiv:1603.06584 [astro-ph.HE].
 - [34] M. Su, T. R. Slatyer, and D. P. Finkbeiner, *Astrophys. J.* **724**, 1044 (2010), arXiv:1005.5480 [astro-ph.HE].
 - [35] M. Ackermann *et al.* (Fermi-LAT), *Astrophys. J.* **793**, 64 (2014), arXiv:1407.7905 [astro-ph.HE].
 - [36] J. Petrovi, P. D. Serpico, and G. Zaharija, *JCAP* **1410**, 052 (2014), arXiv:1405.7928 [astro-ph.HE].
 - [37] M. Lisanti, S. Mishra-Sharma, N. L. Rodd, and B. R. Safdi, (2017), arXiv:1708.09385 [astro-ph.CO].
 - [38] M. Lisanti, S. Mishra-Sharma, N. L. Rodd, B. R. Safdi, and R. H. Wechsler, (2017), arXiv:1709.00416 [astro-ph.CO].
 - [39] A. Albert *et al.* (DES, Fermi-LAT), *Astrophys. J.* **834**, 110 (2017), arXiv:1611.03184 [astro-ph.HE].
 - [40] A. Geringer-Sameth, M. G. Walker, S. M. Koushiappas, S. E. Kuposov, V. Belokurov, G. Torrealba, and N. W. Evans, *Phys. Rev. Lett.* **115**, 081101 (2015), arXiv:1503.02320 [astro-ph.HE].
 - [41] D. Hooper and T. Linden, *JCAP* **1509**, 016 (2015), arXiv:1503.06209 [astro-ph.HE].
 - [42] A. Drlica-Wagner *et al.* (DES, Fermi-LAT), *Astrophys. J.* **809**, L4 (2015), arXiv:1503.02632 [astro-ph.HE].
 - [43] O. Macias, C. Gordon, R. M. Crocker, B. Coleman, D. Paterson, S. Horiuchi, and M. Pohl, (2016), arXiv:1611.06644 [astro-ph.HE].
 - [44] R. Bartels, S. Krishnamurthy, and C. Weniger, *Phys. Rev. Lett.* **116**, 051102 (2016), arXiv:1506.05104 [astro-ph.HE].
 - [45] S. K. Lee, M. Lisanti, and B. R. Safdi, *JCAP* **1505**, 056 (2015), arXiv:1412.6099 [astro-ph.CO].
 - [46] S. K. Lee, M. Lisanti, B. R. Safdi, T. R. Slatyer, and W. Xue, *Phys. Rev. Lett.* **116**, 051103 (2016), arXiv:1506.05124 [astro-ph.HE].
 - [47] T. Linden, N. L. Rodd, B. R. Safdi, and T. R. Slatyer, *Phys. Rev.* **D94**, 103013 (2016), arXiv:1604.01026 [astro-ph.HE].
 - [48] S. Mishra-Sharma, N. L. Rodd, and B. R. Safdi, *Astron. J.* **153**, 253 (2017), arXiv:1612.03173 [astro-ph.HE].
 - [49] S. Horiuchi, M. Kaplinghat, and A. Kwa, *JCAP* **1611**, 053 (2016), arXiv:1604.01402 [astro-ph.HE].
 - [50] F. Acero *et al.* (Fermi-LAT), *Astrophys. J. Suppl.* **218**, 23 (2015), arXiv:1501.02003 [astro-ph.HE].
 - [51] K. M. Gorski, E. Hivon, A. J. Banday, B. D. Wandelt, F. K. Hansen, M. Reinecke, and M. Bartelman, *Astrophys. J.* **622**, 759 (2005), arXiv:astro-ph/0409513 [astro-ph].
 - [52] F. Yusef-Zadeh, J. Hewitt, M. Wardle, V. Tatischeff, D. Roberts, *et al.*, *Astrophys.J.* **762**, 33 (2013), arXiv:1206.6882 [astro-ph.HE].
 - [53] M. Cirelli, G. Corcella, A. Hektor, G. Hutsi, M. Kadastik, *et al.*, *JCAP* **1103**, 051 (2011), arXiv:1012.4515 [hep-ph].
 - [54] K. N. Abazajian and R. E. Keeley, *Phys. Rev.* **D93**, 083514 (2016), arXiv:1510.06424 [hep-ph].
 - [55] L. Zhang, H.-W. Rix, G. van de Ven, J. Bovy, C. Liu, and G. Zhao, *Astrophys. J.* **772**, 108 (2013), arXiv:1209.0256 [astro-ph.GA].
 - [56] M. A. Sanchez-Conde and F. Prada, *Mon. Not. Roy. Astron. Soc.* **442**, 2271 (2014), arXiv:1312.1729 [astro-

- ph.CO].
- [57] N. Klop, F. Zandanel, K. Hayashi, and S. Ando, *Phys. Rev.* **D95**, 123012 (2017), arXiv:1609.03509 [astro-ph.CO].
- [58] K. Hayashi, K. Ichikawa, S. Matsumoto, M. Ibe, M. N. Ishigaki, and H. Sugai, *Mon. Not. Roy. Astron. Soc.* **461**, 2914 (2016), arXiv:1603.08046 [astro-ph.GA].
- [59] V. Bonnivard, C. Combet, D. Maurin, and M. G. Walker, *Mon. Not. Roy. Astron. Soc.* **446**, 3002 (2015), arXiv:1407.7822 [astro-ph.HE].
- [60] Z. Ivezić, A. J. Connolly, J. T. VanderPlass, and A. Gray, *Statistics, Data Mining, and Machine Learning in Astronomy: A Practical Python Guide for the Analysis of Survey Data (Princeton Series in Modern Observational Astronomy)* (Princeton University Press, 2014).
- [61] M. Pato, F. Iocco, and G. Bertone, *JCAP* **1512**, 001 (2015), arXiv:1504.06324 [astro-ph.GA].
- [62] C. F. McKee, A. Parravano, and D. J. Hollenbach, *Astrophys. J.* **814**, 13 (2015), arXiv:1509.05334 [astro-ph.GA].
- [63] A. W. McConnachie, *Astron. J.* **144**, 4 (2012), arXiv:1204.1562 [astro-ph.CO].
- [64] M. Kaplinghat, S. Tulin, and H.-B. Yu, *Phys. Rev. Lett.* **116**, 041302 (2016), arXiv:1508.03339 [astro-ph.CO].